Chinese Science Bulletin

A semi-analytical approach for stiffness modeling of PKM by considering compliance of machine frame with complex geometry

WANG YouYu[1], HUANG Tian[1†], ZHAO XueMan[1], MEI JiangPing[1] & Derek G CHETWYND[2]

[1] School of Mechanical Engineering, Tianjin University, Tianjin 300072, China;
[2] School of Engineering, University of Warwick, Coventry CV4 7AL, UK

Stiffness modeling is one of the most significant issues in the design of parallel kinematic machine (PKM). This paper presents a semi-analytical approach that enables the stiffness of PKM with complex machine frame geometry to be estimated effectively. This approach can be implemented by three steps: (i) decomposition of the entire system into two sub-systems associated with the parallel mechanism and the machine frame respectively; (ii) stiffness modeling of each sub-system using the analytical approach and the finite element analysis; and (iii) generation of the stiffness model of the entire system by means of linear superposition. In the modeling process of each sub-system, the virtual work principle and overall deflection Jacobian are employed with special attention to the bending rigidity of the constrained passive limb and the interface stiffness of the machine frame. The stiffness distribution of a 5-DOF hybrid robot named TriVariant-B is investigated as an example to illustrate the effectiveness of this approach. The contributions of component rigidities to that of the system are evaluated using global indices. It shows that the results achieved by this approach have a good match to those obtained through finite element analysis and experiments.

parallel kinematic machine, stiffness estimation, semi-analytical modeling

Stiffness modeling is one of the most significant issues in the design of parallel kinematic machine since they are mainly designed for implementing high-speed machining and/or forced assembling where high rigidity and high dynamics are crucially required[1]. In principle, the precise stiffness modeling should be accomplished by the finite element analysis (FEA) using commercialized software, particularly for the PKMs whose compliance of machine frame should not be negligible. However, the FEA model has to be re-meshed since the system rigidity varies with the change of configurations, resulting in a very tedious and time-consuming routine. Therefore, a simple yet comprehensive stiffness modeling approach is required in the conceptual design stage that will enable to provide the designers with a guideline prior to the pinpoints.

In the past two decades, a great deal of work has been carried out towards stiffness modeling, analysis and optimization of PKMs. Gosselin[2] seems to be the first to propose a general method to formulate stiffness models of parallel manipulators by merely taking into account the component compliances in actuations. Similar work had been conducted by Clinton et al.[3], EI-Khasawneh et al.[4], Kim et al.[5], Tsai[6], Goldsmith et al.[7] and Joshi et al.[8] amongst others. Recently, taking the Tricept robot as an example, Zhang et al.[9−11] and Wang et al.[12,13] proposed an analytical approach for stiffness modeling of the lower mobility PKM having a passive constraint

Received December 4, 2007; accepted January 7, 2008
doi: 10.1007/s11434-008-0298-1
†Corresponding author (email: htiantju@public.tpt.tj.cn)
Partially supported by the National Natural Science Foundation of China (Grant Nos. 50535010 and 50775158) and the Royal Society UK-China Joint Research Grant (Grant No. IJP-2005/R4)

limb. The FEA and semi-analytical approaches have also been investigated by Corradini et al.[14] and Rizk et al.[15] in dealing with various PKM systems. The modeling methods mentioned above are, however, limited to merely taking into account the component compliances within the parallel mechanisms. Although a substructure-based method[16,17] was proposed for stiffness modeling of a triopod PKM by considering the compliance of beam-like machine frame, it is unsuitable to handle the cases where the machine frame has complex geometry.

This paper presents a semi-analytical approach for the stiffness modeling of the PKM having complex machine frame geometry. In this approach, the PKM is decomposed into two sub-systems associated with the parallel mechanism and the machine frame. The stiffness model of each sub-system is formulated in such a way that the components in the other are assumed to be rigid. The stiffness model of the parallel mechanism is generated using the analytical approach while that of the machine frame is formulated using the static condensation of a FEA model. Finally the stiffness model of the entire system is achieved by linear superposition using the interface compatibility conditions. Stiffness evaluation of the TriVariant-B robot[18,19] is carried out as an example to illustrate the effectiveness of this approach and the results are compared with those obtained through finite element analysis and experiments.

1 General theory

Figure 1 shows the schematic diagram of a general PKM composed of a platform and a machine frame (base) connected by limbs through joints. From the substructure synthesis point of view, the PKM can be divided into two subsystems, i.e. the parallel mechanism and the machine frame with the base-connected joints being the

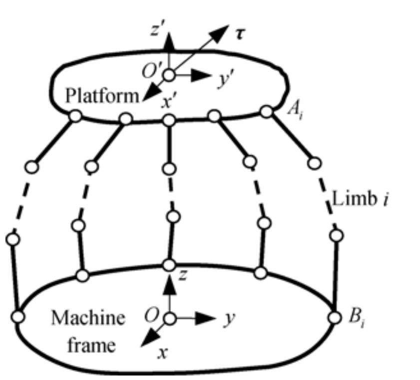

Figure 1 Schematic diagram of a PKM.

interfaces in between. Therefore, the stiffness model of the entire system can be achieved by two steps: (i) formulation of the stiffness model of a subsystem by assuming that the other is rigid; and (ii) linear superposition of the deflections of two subsystems produced by the same external load imposed on the platform.

In the stiffness modeling of the parallel mechanism, assume that the machine frame and the platform are rigid for the time being and use subscript "*m*" to represent the machine frame. Let $\boldsymbol{\tau}$ be the externally applied wrench imposed on the platform at point O' and let $\boldsymbol{\Delta}_m$ be the corresponding deflection twist in terms of translation and rotation due to flexibilities of the components within the limbs. The virtual work principle gives

$$\boldsymbol{\tau}^{\mathrm{T}}\boldsymbol{\Delta}_m = \boldsymbol{f}^{\mathrm{T}}\Delta\boldsymbol{\rho}\,, \tag{1}$$

where $\boldsymbol{f}$ and $\Delta\boldsymbol{\rho}$ represent the generalized forces and deflections at the interface between the limbs and the platform, respectively. On one hand, $\boldsymbol{\Delta}_m$ and $\Delta\boldsymbol{\rho}$ can be linked by

$$\Delta\boldsymbol{\rho} = \boldsymbol{J}_m\boldsymbol{\Delta}_m\,, \tag{2}$$

where $\boldsymbol{J}_m$ is a 6×6 matrix known as the *overall deflection Jacobian* of the mechanism, mapping $\boldsymbol{\Delta}_m$ into $\Delta\boldsymbol{\rho}$ provided that the machine frame is rigid. On the other hand, the Hooke's law gives

$$\boldsymbol{f} = \overline{\boldsymbol{K}}_m\Delta\boldsymbol{\rho}\,, \tag{3}$$

where $\overline{\boldsymbol{K}}_m$ is a 6×6 positive definite matrix known as the component stiffness matrix of the parallel mechanism. Substituting eqs. (2) and (3) into eq. (1) results in

$$\boldsymbol{\tau} = \boldsymbol{K}_m\boldsymbol{\Delta}_m\,, \tag{4}$$

where $\boldsymbol{K}_m = \boldsymbol{J}_m^{\mathrm{T}}\overline{\boldsymbol{K}}_m\boldsymbol{J}_m$ is defined as the stiffness matrix of the parallel mechanism at point O'.

In the stiffness modeling of the machine fame, assume that the limbs within the parallel mechanism are rigid for the time being and use subscript "*f*" to represent the machine frame. Let $\boldsymbol{\Delta}_f$ be the deflection twist due to the flexibility of the machine frame produced by $\boldsymbol{\tau}$. The virtual work principle leads to

$$\boldsymbol{\tau}^{\mathrm{T}}\boldsymbol{\Delta}_f = \boldsymbol{f}^{\mathrm{T}}\Delta\boldsymbol{\rho}\,. \tag{5}$$

In this case, $\boldsymbol{f}$ and $\Delta\boldsymbol{\rho}$ should be understood as the generalized force and corresponding deflection at the interface between the limbs and the machine frame. Similarly, $\Delta\boldsymbol{\rho}$ relates $\boldsymbol{\Delta}_f$ by

$$\Delta\boldsymbol{\rho} = \boldsymbol{J}_f\boldsymbol{\Delta}_f\,, \tag{6}$$

where $\boldsymbol{J}_f$ represents the *overall deflection Jacobian* of the machine frame, mapping $\boldsymbol{\Delta}_f$ into $\Delta\boldsymbol{\rho}$ provided that the limbs within the parallel mechanism are rigid. The Hooke's law yields

$$\boldsymbol{f} = \overline{\boldsymbol{K}}_f \Delta\boldsymbol{\rho}, \tag{7}$$

where $\overline{\boldsymbol{K}}_f$ is a positive definite matrix known as the component stiffness matrix of the machine frame. Substituting eqs. (6) and (7) into eq. (5) results in

$$\boldsymbol{\tau} = \boldsymbol{K}_f \boldsymbol{\Delta}_f. \tag{8}$$

As a counterpart of $\boldsymbol{K}_m$, $\boldsymbol{K}_f = \boldsymbol{J}_f^{\mathrm{T}} \overline{\boldsymbol{K}}_f \boldsymbol{J}_f$ is defined as the stiffness matrix of the machine frame at point O'.

At this stage, the stiffness model of the PKM as a whole can be achieved by linear superposition since two subsystems are linear in nature, i.e.

$$\boldsymbol{\tau} = \boldsymbol{K}\boldsymbol{\Delta}, \tag{9}$$

where

$$\boldsymbol{\Delta} = \boldsymbol{\Delta}_m + \boldsymbol{\Delta}_f, \quad \boldsymbol{K}^{-1} = \boldsymbol{K}_m^{-1} + \boldsymbol{K}_f^{-1}.$$

In what follows, we will take the 2-DOF spherical parallel mechanism and the machine frame of the TriVariant-B robot shown in Figure 2 as an example to develop $\boldsymbol{J}_m$, $\boldsymbol{J}_f$, $\overline{\boldsymbol{K}}_m$ and $\overline{\boldsymbol{K}}_f$.

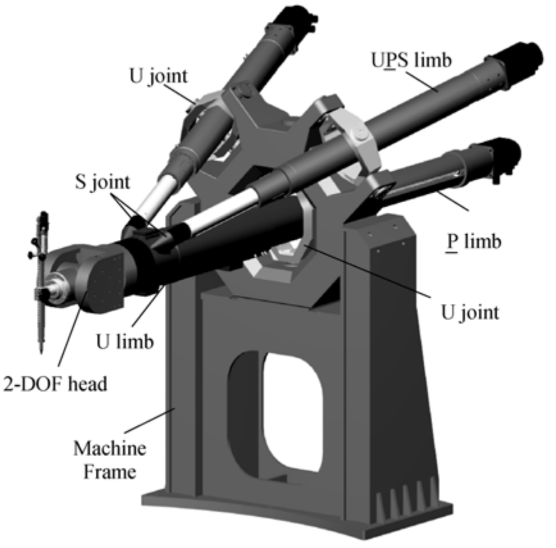

Figure 2 The TriVariant-B.

2 System description of the TriVariant-B robot

As shown in Figure 2, the TriVariant-B[19] is a 5-DOF hybrid robot which is essentially composed of a 2-DOF spherical parallel mechanism (SPM) and a 3-DOF open-loop kinematic chain (OKC). The robot is mounted on a modularized machine frame. The SPM consists of a properly constrained passive limb (U limb) and two identical unconstrained active limbs (UPS limb). One end of the U limb is rigidly fixed to the inner ring of a U joint connected to the machine frame, and the other end connected to two identical UPS limbs. The 3-DOF OKC consists of an active long tube (P limb) and a 2-DOF rotating head attached to one extremity of the tube. The P limb is linked with the U limb by a prismatic joint. Here, U, P and S represent respectively universal, prismatic and spherical joints and underlined P denotes an active prismatic joint driven by a servomotor.

Figure 3 shows the schematic diagram of the 2-DOF SPM. $B_i (i=1,2,3)$ represents the center of the U joint connecting the limb i to the machine frame. For convenience, all B_i are taken to lie within a plane that has a tilt angle ϕ with the horizontal plane. $A_i (i=1,2)$ is the center of the spherical joint of the ith UPS limb and A_3 the intersection of the axial axis of the limb 3 (U limb) with its normal plane, in which all A_i are placed. Establish the reference coordinate system $B_3 - x_3 y_3 z_3$ with the rotation axis of its outer ring being the y_3 axis and the z_3 axis being placed vertically downwards as shown. Using the same rule, the reference coordinate systems $B_i - x_i y_i z_i$ associated with limb i (i=1,2) are similarly placed with the z_i axis being vertically downwards and the y_i axis being parallel to $\overline{B_3 B'_i}$. Meanwhile, the body-fixed coordinate systems $B_i - u_i v_i w_i$ $(i=1,2,3)$ are also placed

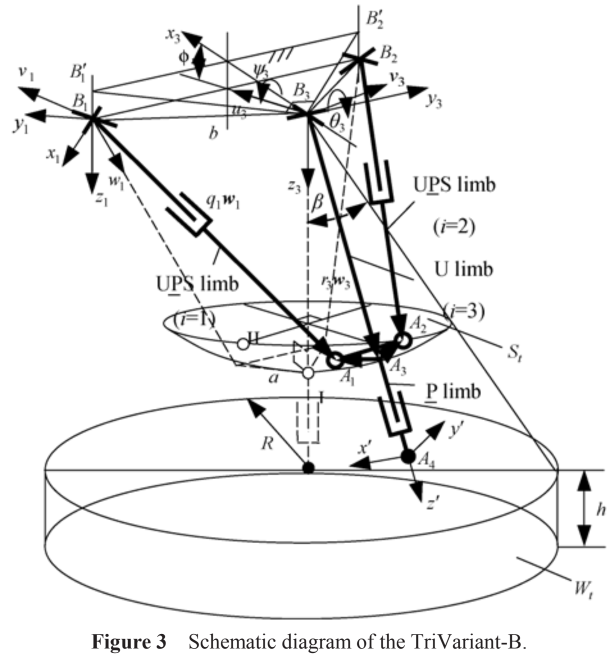

Figure 3 Schematic diagram of the TriVariant-B.

where the u_i ($i=1,2,3$) axis is coincident with the inner ring's rotational axis of the U joint, the w_i axis is coincident with the axial axis of the limb and the v_i axis satisfies the right hand rule. Here, we define u_i, v_i and $\boldsymbol{w}_i$ as the unit vectors of u_i, v_i and w_i axes, respectively. The task workspace of the TriVariant-B, denoted by W_t, is a cylinder of radius R and height h, the task workspace of the 2-DOF SPM, denoted by S_t, is a spherical surface of radius r_3 bounded by the half conical angle β as shown in Figure 3.

3 Formulation of the overall deflection Jacobian

3.1 Formulation of $\boldsymbol{J}_m$

As shown in Figure 3, the position vector $r_3 = (x \quad y \quad z)^{\mathrm{T}}$ of the reference point A_3 located at the extremity of the U limb (the platform) can be represented by either or two ways

$$\boldsymbol{r}_3 = \boldsymbol{b}_i + q_i \boldsymbol{w}_i - \boldsymbol{a}_i, \quad i=1,2, \tag{10}$$

$$\boldsymbol{r}_3 = r_3 \boldsymbol{w}_3, \tag{11}$$

where r_3 is the length of the axial axis of the U limb; q_i is the length of the axial axes of the U$\underline{\text{P}}$S limb i(i = 1, 2); $\boldsymbol{a}_i = \boldsymbol{R}_3 \boldsymbol{a}_{i0}$, $\boldsymbol{a}_{i0}$ and $\boldsymbol{b}_i$ are the constant position vectors of A_i and B_i measured in $A_3 - u_3 v_3 w_3$ and $B_3 - x_3 y_3 z_3$, and $\boldsymbol{R}_3$ is the orientation matrix of $A_3 - u_3 v_3 w_3$ with respect to $B_3 - x_3 y_3 z_3$.

Assume that the machine frame is rigid. Taking small perturbation of eqs. (10) and (11) leads to

$$\boldsymbol{\Delta}_p = \Delta q_i \boldsymbol{w}_i + q_i \boldsymbol{\Delta}_{\alpha i} \times \boldsymbol{w}_i - \boldsymbol{\Delta}_\alpha \times \boldsymbol{a}_i, \quad i=1,2, \tag{12}$$

$$\boldsymbol{\Delta}_p - \boldsymbol{\Delta}'_p = r_3 \left(\boldsymbol{\Delta}_\alpha - \boldsymbol{\Delta}'_\alpha\right) \times \boldsymbol{w}_3, \tag{13}$$

where Δq_i $(i=1,2)$ is the tensile deflection at point A_i along the axial axis of U$\underline{\text{P}}$S limb i, $\boldsymbol{\Delta}_{\alpha i}$ is the rotational deflection vector of U$\underline{\text{P}}$S limb i; $\boldsymbol{\Delta}_p$ and $\boldsymbol{\Delta}_\alpha$ are the translational and the rotational deflections at point A_3 with $\boldsymbol{\Delta}'_p$ and $\boldsymbol{\Delta}'_\alpha$ being those by merely considering the compliance of the U limb.

Taking dot product with $\boldsymbol{w}_i$ on both sides of eq. (12) leads to

$$\Delta q_i = \boldsymbol{w}_i^{\mathrm{T}} \boldsymbol{\Delta}_p + \left(\boldsymbol{a}_i \times \boldsymbol{w}_i\right)^{\mathrm{T}} \boldsymbol{\Delta}_\alpha. \tag{14}$$

In $A_3 - u_3 v_3 w_3$, $\boldsymbol{\Delta}'_p$ and $\boldsymbol{\Delta}'_\alpha$ can be expressed as

$$\boldsymbol{\Delta}'_p = \Delta p_u \boldsymbol{u}_3 + \Delta p_v \boldsymbol{v}_3 + \Delta p_w \boldsymbol{w}_3,,$$

$$\boldsymbol{\Delta}'_\alpha = \Delta\alpha_u \boldsymbol{u}_3 + \Delta\alpha_v \boldsymbol{v}_3 + \Delta\alpha_w \boldsymbol{w}_3, \tag{15}$$

where $\Delta p_{u(v)}$ and $\Delta\alpha_{u(v)}$ are the bending deflections (slopes) of the U limb at point A_3 along (about) the $u_3(v_3)$ axes; and $\Delta p_w(\Delta\alpha_w)$ is the axial (torsional) deflection along (about) the w_3 axis of the U limb at point A_3. Substituting eq. (15) into eq. (13) and taking dot product with $\boldsymbol{u}_3$, $\boldsymbol{v}_3$ and $\boldsymbol{w}_3$ on both sides of eq. (13) leads to

$$\boldsymbol{u}_3^{\mathrm{T}} \boldsymbol{\Delta}_p - r_3 \boldsymbol{v}_3^{\mathrm{T}} \boldsymbol{\Delta}_\alpha = \Delta p_u - r_3 \Delta\alpha_v, \tag{16}$$

$$\boldsymbol{v}_3^{\mathrm{T}} \boldsymbol{\Delta}_p + r_3 \boldsymbol{u}_3^{\mathrm{T}} \boldsymbol{\Delta}_\alpha = \Delta p_v + r_3 \Delta\alpha_u, \tag{17}$$

$$\boldsymbol{w}_3^{\mathrm{T}} \boldsymbol{\Delta}_p = \Delta p_w. \tag{18}$$

Note that the constraints imposed by the U joint of the U limb prevent any rotation about an axis perpendicular to the plane (instantaneously) containing the axes of its inner and outer rings. Thus

$$\boldsymbol{n}^{\mathrm{T}} \left(\boldsymbol{\Delta}_\alpha - \boldsymbol{\Delta}'_\alpha\right) = 0, \tag{19}$$

where $\boldsymbol{n} = \boldsymbol{u}'_3 \times \boldsymbol{v}_3$ and $\boldsymbol{u}'_3$ is the unit vector of the rotation axis of the outer ring of the U limb. Because the U limb is a beam-like component, its bending deflections and slopes are dependent. It can be proved that the following relationship holds by taking into account the compatibility conditions provided by the loop-closure equations (see Section 4.1.2)

$$\begin{pmatrix} \Delta\alpha_u \\ \Delta\alpha_v \end{pmatrix} = \boldsymbol{B} \begin{pmatrix} \Delta r_u \\ \Delta r_v \end{pmatrix}, \ \boldsymbol{B} = \begin{bmatrix} b_{11} & b_{12} \\ b_{21} & b_{22} \end{bmatrix}. \tag{20}$$

Substituting eq. (20) into eqs. (14)—(19) and rewriting in matrix form yields

$$\Delta\boldsymbol{\rho} = \boldsymbol{J}_m \boldsymbol{\Delta}_m, \tag{21}$$

where

$$\boldsymbol{\Delta}_m = \begin{pmatrix} \boldsymbol{\Delta}_p \\ \boldsymbol{\Delta}_\alpha \end{pmatrix}, \ \Delta\boldsymbol{\rho} = \begin{pmatrix} \Delta\boldsymbol{\rho}_a \\ \Delta\boldsymbol{\rho}_c \end{pmatrix}, \ \Delta\boldsymbol{\rho}_a = \begin{pmatrix} \Delta q_1 \\ \Delta q_2 \end{pmatrix},$$

$$\Delta\boldsymbol{\rho}_c = \left(\Delta p_w \quad \Delta p_u \quad \Delta p_v \quad \Delta\alpha_w\right)^{\mathrm{T}},$$

$$\boldsymbol{J}_m = \begin{bmatrix} \boldsymbol{J}_a \\ \boldsymbol{J}_c \end{bmatrix}, \ \boldsymbol{J}_a = \begin{bmatrix} \boldsymbol{w}_1^{\mathrm{T}} & \left(\boldsymbol{a}_1 \times \boldsymbol{w}_1\right)^{\mathrm{T}} \\ \boldsymbol{w}_2^{\mathrm{T}} & \left(\boldsymbol{a}_2 \times \boldsymbol{w}_2\right)^{\mathrm{T}} \end{bmatrix}, \ \boldsymbol{J}_c = \boldsymbol{T}_c^{-1} \boldsymbol{J}_{cv},$$

$$\boldsymbol{J}_{cv} = \begin{bmatrix} \boldsymbol{w}_3^{\mathrm{T}} & \boldsymbol{0}_{1\times 3} \\ \boldsymbol{u}_3^{\mathrm{T}} & -r_3 \boldsymbol{v}_3^{\mathrm{T}} \\ \boldsymbol{v}_3^{\mathrm{T}} & r_3 \boldsymbol{u}_3^{\mathrm{T}} \\ \boldsymbol{0}_{1\times 3} & \boldsymbol{n}^{\mathrm{T}} \end{bmatrix},$$

$$\boldsymbol{T}_c = \begin{bmatrix} 1 & 0 & 0 & 0 \\ 0 & 1-r_3 b_{21} & -r_3 b_{22} & 0 \\ 0 & r_3 b_{11} & 1+r_3 b_{12} & 0 \\ 0 & b_{11}\boldsymbol{n}^{\mathrm{T}}\boldsymbol{u}_3 & b_{12}\boldsymbol{n}^{\mathrm{T}}\boldsymbol{u}_3 & \boldsymbol{n}^{\mathrm{T}}\boldsymbol{w}_3 \end{bmatrix}.$$

Referring to the terminology defined by Joshi et al.[20], $\boldsymbol{J}_a$ is known as the *deflection Jacobian of actuations* of the SPM because each row in $\boldsymbol{J}_a$ represents a unit wrench of actuations imposed to an unconstrained active UPS limb. As a counterpart of $\boldsymbol{J}_a$, $\boldsymbol{J}_c$ is known as the *deflection Jacobian of constraints* of the SPM because each row in $\boldsymbol{J}_c$ represents a unit wrench of constraints imposed on the properly constrained passive U limb. Obviously, $\boldsymbol{J}_m$ is the *overall deflection Jacobian* of the SPM defined in eq. (2).

3.2 Formulation of $\boldsymbol{J}_f$

On a dual part of the development of $\boldsymbol{J}_m$, assume that the SPM is rigid. Taking small perturbation of eqs. (10) and (11) leads to

$$\boldsymbol{\Delta}_p = \Delta\boldsymbol{p}_i + \Delta\boldsymbol{\alpha}_i \times \boldsymbol{b}_i + q_i \Delta\boldsymbol{\alpha}_i \times \boldsymbol{w}_i - \boldsymbol{\Delta}_\alpha \times \boldsymbol{a}_i, \quad i=1,2, \tag{22}$$

$$\boldsymbol{\Delta}_p = \Delta\boldsymbol{p}_3 + r_3 \boldsymbol{\Delta}_\alpha \times \boldsymbol{w}_3, \tag{23}$$

where $\Delta\boldsymbol{p}_i$ and $\Delta\boldsymbol{\alpha}_i$ are the translational and the rotational deformations of the machine frame at point $B_i\ (i=1,2,3)$.

Taking dot products with $\boldsymbol{w}_i\ (i=1,2)$ on both sides of eq. (22) yields

$$\boldsymbol{w}_i^{\mathrm{T}}\boldsymbol{\Delta}_p + (\boldsymbol{a}_i \times \boldsymbol{w}_i)^{\mathrm{T}}\boldsymbol{\Delta}_\alpha = \boldsymbol{w}_i^{\mathrm{T}}\Delta\boldsymbol{p}_i + (\boldsymbol{b}_i \times \boldsymbol{w}_i)^{\mathrm{T}}\Delta\boldsymbol{\alpha}_i, \quad i=1,2. \tag{24}$$

Again, taking dot product with $\boldsymbol{u}_3$, $\boldsymbol{v}_3$ and $\boldsymbol{w}_3$, respectively, on both sides of eq. (23) leads to

$$\boldsymbol{u}_3^{\mathrm{T}}\boldsymbol{\Delta}_p - r_3\boldsymbol{v}_3^{\mathrm{T}}\boldsymbol{\Delta}_\alpha = \boldsymbol{u}_3^{\mathrm{T}}\Delta\boldsymbol{p}_3, \tag{25}$$

$$\boldsymbol{v}_3^{\mathrm{T}}\boldsymbol{\Delta}_p + r_3\boldsymbol{u}_3^{\mathrm{T}}\boldsymbol{\Delta}_\alpha = \boldsymbol{v}_3^{\mathrm{T}}\Delta\boldsymbol{\alpha}_3, \tag{26}$$

$$\boldsymbol{w}_3^{\mathrm{T}}\boldsymbol{\Delta}_p = \boldsymbol{w}_3^{\mathrm{T}}\Delta\boldsymbol{p}_3. \tag{27}$$

Utilizing the similar procedure to formulate eq. (19) gives

$$\boldsymbol{n}^{\mathrm{T}}\boldsymbol{\Delta}_\alpha = \boldsymbol{n}^{\mathrm{T}}\Delta\boldsymbol{\alpha}_3. \tag{28}$$

Rewriting eqs. (24)—(28) in matrix form finally results in

$$\Delta\boldsymbol{\rho} = \boldsymbol{J}_f \boldsymbol{\Delta}_f, \tag{29}$$

where

$$\boldsymbol{\Delta}_f = \begin{pmatrix} \boldsymbol{\Delta}_p \\ \boldsymbol{\Delta}_\alpha \end{pmatrix},\ \Delta\boldsymbol{\rho} = \begin{pmatrix} \Delta\boldsymbol{\rho}_a \\ \Delta\boldsymbol{\rho}_c \end{pmatrix},\ \Delta\boldsymbol{\rho}_a = \begin{pmatrix} \Delta\boldsymbol{\rho}_1 \\ \Delta\boldsymbol{\rho}_2 \end{pmatrix},$$

$$\Delta\boldsymbol{\rho}_c = \Delta\boldsymbol{\rho}_3,\ \Delta\boldsymbol{\rho}_i = \begin{pmatrix} \Delta\boldsymbol{p}_i \\ \Delta\boldsymbol{\alpha}_i \end{pmatrix},\ i=1,2,3,$$

$$\boldsymbol{J}_f = \boldsymbol{J}'^{+}\begin{bmatrix} \boldsymbol{J}_a \\ \boldsymbol{J}_{cv} \end{bmatrix},\ \boldsymbol{J}' = \begin{bmatrix} \boldsymbol{J}'_a & \boldsymbol{0}_{2\times 6} \\ \boldsymbol{0}_{4\times 12} & \boldsymbol{J}'_c \end{bmatrix},$$

$$\boldsymbol{J}'^{+} = \left[\boldsymbol{J}'^{\mathrm{T}}\boldsymbol{J}'\right]^{-1}\boldsymbol{J}'^{\mathrm{T}},$$

$$\boldsymbol{J}'_a = \begin{bmatrix} \boldsymbol{w}_1^{\mathrm{T}} & (\boldsymbol{b}_1 \times \boldsymbol{w}_1)^{\mathrm{T}} & \boldsymbol{0}_{1\times 6} & \\ & \boldsymbol{0}_{1\times 6} & \boldsymbol{w}_2^{\mathrm{T}} & (\boldsymbol{b}_2 \times \boldsymbol{w}_2)^{\mathrm{T}} \end{bmatrix},$$

$$\boldsymbol{J}'_c = \begin{bmatrix} \boldsymbol{w}_3^{\mathrm{T}} & \boldsymbol{0}_{1\times 3} \\ \boldsymbol{u}_3^{\mathrm{T}} & \boldsymbol{0}_{1\times 3} \\ \boldsymbol{v}_3^{\mathrm{T}} & \boldsymbol{0}_{1\times 3} \\ \boldsymbol{0}_{1\times 3} & \boldsymbol{n}^{\mathrm{T}} \end{bmatrix}.$$

As the counterpart of $\boldsymbol{J}_m$, $\boldsymbol{J}_f$ is the *overall deflection Jacobian* of the machine frame defined in eq. (6).

4 Formulation of the component stiffness matrices

4.1 Formulation of $\overline{\boldsymbol{K}}_m$

As the dual part of $\Delta\boldsymbol{\rho}$ in eq. (21), $\boldsymbol{f}$ in eq. (1) can be considered as a set of *generalized* forces by which the work done on $\Delta\boldsymbol{\rho}$ is equal to that done by $\boldsymbol{\tau}$ on $\boldsymbol{\Delta}_m$. Note that $\Delta\boldsymbol{\rho}$ and $\boldsymbol{f}$ have two dual subsets, i.e. ($\Delta\boldsymbol{\rho}_a$, $\boldsymbol{f}_a$) and ($\Delta\boldsymbol{\rho}_c$, $\boldsymbol{f}_c$), associated respectively with the actuations and constraints of the SPM. Consequently, $\boldsymbol{f}_a$ and $\boldsymbol{f}_c$ can be defined as

$$\boldsymbol{f}_a = (f_{a1} \quad f_{a2})^{\mathrm{T}},\ \boldsymbol{f}_c = (f_{cw} \quad f_{cu} \quad f_{cv} \quad f_{ct})^{\mathrm{T}}, \tag{30}$$

where f_{ai} (i=1,2) is the axial actuation force imposed at point A_i along the z_i axis of the ith UPS limb; f_{cw} is the axial constraint force imposed at point A_3 along the w_3 axis of the U limb; f_{ct} is the constraint torque imposed at A_3 about the w_3 axis; f_{cu} and f_{cv} are the *generalized* constraint forces imposed at A_3 along the u_3 and v_3 axes. The term '*generalized*' here means that the total work done by f_{cu} on Δp_u and f_{cv} on Δp_v is equivalent to the elastic bending energy of the U limb. Thus, eq. (3) can be written in partition form as

$$f_a = K_a \Delta \rho_a, \quad f_c = K_c \Delta \rho_c, \quad \bar{K}_m = \begin{bmatrix} K_a & \\ & K_c \end{bmatrix}, \quad (31)$$

where K_a and K_c are defined as the *component stiffness matrices of actuations and constraints* of the SPM, respectively. For this particular problem, the elements in K_a and K_c will be developed in depth in the next section.

Modeling of K_a

K_a given in eq. (31) has simply a diagonal form

$$K_a = \begin{bmatrix} k_{a1} & \\ & k_{a2} \end{bmatrix}, \quad (32)$$

where k_{ai} is the axial stiffness coefficient of the ith U<u>P</u>S limb. As shown in Figure 4, k_{ai} can be modeled by a set of serially connected springs such that

$$k_{ai}^{-1} = \sum_{j=1}^{7} k_{aij}^{-1}, \quad i = 1, 2, \quad (33)$$

where k_{aij} $(j = 1, \cdots, 7)$ is the axial stiffness coefficient of the jth component, sequentially numbered by 1) S joint, 2) rod, 3) nut, 4) lead screw, 5) rear bearing, 6) segment of the limb body from the rear bearing to the U joint, and 7) U joint. Note that k_{ai2}, k_{ai3}, k_{ai5} and k_{ai6} are constants. k_{ai1}, k_{ai4} and k_{ai7} are configuration dependent as addressed in ref. [13].

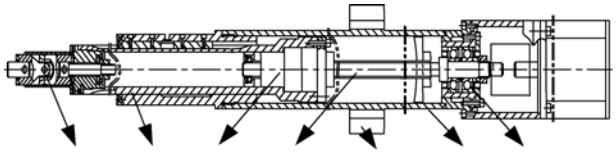

Figure 4 Mechanical structure of the U<u>P</u>S limb.

Modeling of K_c

K_c given in eq. (31) can be written in a partitioned form as

$$K_c = \begin{bmatrix} k_{ca} & & \\ & K_{cb} & \\ & & k_{ct} \end{bmatrix}, \quad (34)$$

where K_{cb} is a 2×2 matrix known as the *generalized* bending stiffness matrix at the extremity of the U limb; $k_{ca}(k_{ct})$ is the axial (torsional) stiffness coefficient along (about) the w_3 axis at the extremity of the U limb.

As shown in Figure 5, k_{ca} and k_{ct} can be modeled by

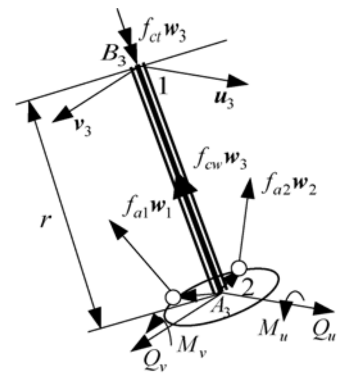

Figure 5 Schematic diagram of U limb.

$$k_{ca}^{-1} = \sum_{i=1}^{2} k_{cai}^{-1}, \quad k_{ct}^{-1} = \sum_{i=1}^{2} k_{cti}^{-1}, \quad (35)$$

where $k_{caj}(k_{cti})$ $(i = 1, 2)$ is the axial (torsional) stiffness coefficient of the limb body and U joint along (about) the axial axis of the U limb and can be obtained using the method given in ref. [13].

In order to formulate K_{cb}, consider the U limb as a beam element whose bending deflections are the only concerns. Therefore, eliminate the rigid body motions produced by compliances of the U<u>P</u>S limbs together with the tensile deformation along and the torsional deformation about the w_3 axis for the time being while keeping the $A_3 - u_3 v_3 w_3$ coordinate conventions unchanged. Then, K_{cb} can be modeled by two steps as follows.

(i) Energy equivalence principle. As shown in Figure 5, the *generalized* force $f_{cu(v)}$ can be defined in such a way that the total work done by $f_{cu(v)}$ on $\Delta p_{u(v)}$ should be equal to that done by all *real* reaction forces (moments) on the corresponding elastic bending deflections (slopes) at point A_3 of the U limb. Thus, the virtual work principle states

$$\begin{pmatrix} \Delta p_u \\ \Delta p_v \end{pmatrix}^{\mathrm{T}} \begin{pmatrix} f_{cu} \\ f_{cv} \end{pmatrix} = \begin{pmatrix} \Delta p_u \\ \Delta p_v \\ \Delta \alpha_u \\ \Delta \alpha_v \end{pmatrix}^{\mathrm{T}} \begin{pmatrix} Q_u \\ Q_v \\ M_u \\ M_v \end{pmatrix}, \quad (36)$$

where $\Delta p_{u(v)}$ and $Q_{u(v)}$ are the deflection and shearing force along the $u_3(v_3)$ axis, $\Delta \alpha_{v(u)}$ and $M_{u(v)}$ are the slope and moment about the $u_3(v_3)$ axis at point A_3 of the U limb. Hooke's law gives

$$\begin{pmatrix} Q_u \\ Q_v \\ M_u \\ M_v \end{pmatrix} = \overline{\boldsymbol{K}}_e \begin{pmatrix} \Delta p_u \\ \Delta p_v \\ \Delta\alpha_u \\ \Delta\alpha_v \end{pmatrix}, \tag{37}$$

where $\overline{\boldsymbol{K}}_e$ is a 4×4 stiffness matrix of the beam element when the boundary conditions at the U joint of the U limb are specified[13]. Also, keep in mind that

$$\begin{pmatrix} f_{cu} \\ f_{cv} \end{pmatrix} = \boldsymbol{K}_{cb} \begin{pmatrix} \Delta p_u \\ \Delta p_v \end{pmatrix}. \tag{38}$$

Substituting eqs. (37) and (38) into eq. (36) leads to

$$\begin{pmatrix} \Delta p_u \\ \Delta p_v \end{pmatrix}^{\mathrm{T}} \boldsymbol{K}_{cb} \begin{pmatrix} \Delta p_u \\ \Delta p_v \end{pmatrix} = \begin{pmatrix} \Delta p_u \\ \Delta p_v \\ \Delta\alpha_u \\ \Delta\alpha_v \end{pmatrix}^{\mathrm{T}} \overline{\boldsymbol{K}}_e \begin{pmatrix} \Delta p_u \\ \Delta p_v \\ \Delta\alpha_u \\ \Delta\alpha_v \end{pmatrix}. \tag{39}$$

(ii) Compatibility conditions. Since the rigid body motions together with the tensile and torsional deflections of the U limb have been eliminated, the deflection twist at point A_3 should comply with a set of compatibility conditions given as follows (see also eqs. (14) and (18))

$$\boldsymbol{w}_i^{\mathrm{T}} \boldsymbol{\Delta}_p + (\boldsymbol{a}_i \times \boldsymbol{w}_i)^{\mathrm{T}} \boldsymbol{\Delta}_\alpha = 0, \quad i = 1,2, \tag{40}$$

$$\boldsymbol{w}_3^{\mathrm{T}} \boldsymbol{\Delta}_p = 0. \tag{41}$$

Note that $\boldsymbol{\Delta}_p$ and $\boldsymbol{\Delta}_\alpha$ here should be understood as the small translational and rotational deflections at point A_3, merely produced by the bending compliance of the U limb. Thus

$$\boldsymbol{\Delta}_p = [\boldsymbol{u}_3 \quad \boldsymbol{v}_3 \quad \boldsymbol{w}_3] \begin{pmatrix} \Delta p_u \\ \Delta p_v \\ 0 \end{pmatrix} = [\boldsymbol{u}_3 \quad \boldsymbol{v}_3] \begin{pmatrix} \Delta p_u \\ \Delta p_v \end{pmatrix},$$

$$\boldsymbol{\Delta}_\alpha = [\boldsymbol{u}_3 \quad \boldsymbol{v}_3 \quad \boldsymbol{w}_3] \begin{pmatrix} \Delta \alpha_u \\ \Delta \alpha_v \\ 0 \end{pmatrix} = [\boldsymbol{u}_3 \quad \boldsymbol{v}_3] \begin{pmatrix} \Delta \alpha_u \\ \Delta \alpha_v \end{pmatrix}. \tag{42}$$

Substituting eq. (42) into eqs. (40) and (41) gives

$$\begin{pmatrix} \Delta\alpha_u \\ \Delta\alpha_v \end{pmatrix} = \boldsymbol{B} \begin{pmatrix} \Delta p_u \\ \Delta p_v \end{pmatrix}, \tag{43}$$

where

$$\boldsymbol{B} = -\boldsymbol{B}_\alpha^{+} \boldsymbol{B}_p = \begin{bmatrix} b_{11} & b_{12} \\ b_{21} & b_{22} \end{bmatrix},$$

$$\boldsymbol{B}_p = [\boldsymbol{w}_1 \quad \boldsymbol{w}_2 \quad \boldsymbol{w}_3]^{\mathrm{T}} [\boldsymbol{u}_3 \quad \boldsymbol{v}_3],$$

$$\boldsymbol{B}_\alpha = [\boldsymbol{a}_1 \times \boldsymbol{w}_1 \quad \boldsymbol{a}_2 \times \boldsymbol{w}_2 \quad \boldsymbol{0}]^{\mathrm{T}} [\boldsymbol{u}_3 \quad \boldsymbol{v}_3],$$

$$\boldsymbol{B}_\alpha^{+} = \left(\boldsymbol{B}_\alpha^{\mathrm{T}} \boldsymbol{B}_\alpha\right)^{-1} \boldsymbol{B}_\alpha^{\mathrm{T}}.$$

At this stage, $\boldsymbol{B}$ in eq. (20) has been determined. Substituting eq. (43) into eq. (39), we can finally obtain

$$\boldsymbol{K}_{cb} = \begin{bmatrix} \boldsymbol{E}_2 \\ \boldsymbol{B} \end{bmatrix}^{\mathrm{T}} \overline{\boldsymbol{K}}_e \begin{bmatrix} \boldsymbol{E}_2 \\ \boldsymbol{B} \end{bmatrix}, \tag{44}$$

where $\boldsymbol{E}_2$ denotes a unit matrix of order 2. It is worthwhile pointing out that the *generalized force*, $f_{cu(v)}$, can be visualized as the projection of the constraint wrench of the U limb onto the $u_3(v_3)$ axis. This also explains why $\boldsymbol{K}_{cb}$ should be modeled by non-diagonal matrix rather than by two lumped springs as recommended by refs. [9—11].

4.2 Formulation of $\overline{\boldsymbol{K}}_f$

In order to determine $\overline{\boldsymbol{K}}_f$, let $\boldsymbol{K}_g$ be the global stiffness of the machine frame whose FEA model is shown in Figure 6. The static equilibrium equation of the machine frame can then be written in partition form

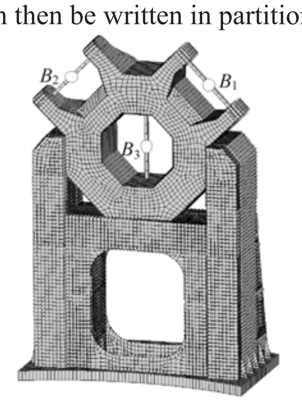

Figure 6 The FEA model.

$$\begin{bmatrix} \boldsymbol{p}_a \\ \boldsymbol{0} \end{bmatrix} = \begin{bmatrix} \boldsymbol{K}_{gaa} & \boldsymbol{K}_{gba} \\ \boldsymbol{K}_{gab} & \boldsymbol{K}_{gbb} \end{bmatrix} \begin{bmatrix} \boldsymbol{\delta}_a \\ \boldsymbol{\delta}_b \end{bmatrix}, \tag{45}$$

where $\boldsymbol{p}_a$ ($\boldsymbol{p}_a = \boldsymbol{f}$) is the load vector exerted on the machine frame at the interface nodes (see Figure 6); $\boldsymbol{\delta}_a$ ($\boldsymbol{\delta}_a = \Delta\boldsymbol{\rho}$) and $\boldsymbol{\delta}_b$ are the displacement vectors at the interface and interior nodes of the machine frame, respectively. Eq. (45) can then be rewritten using the static condensation technique available in structural mechanics

$$\boldsymbol{p}_a = \overline{\boldsymbol{K}}_f \boldsymbol{\delta}_a = \sum_{i=1}^{3} \overline{\boldsymbol{K}}_{fi} \boldsymbol{\delta}_{ai}, \tag{46}$$

where

$$\overline{\boldsymbol{K}}_f = \boldsymbol{K}_{gaa} - \boldsymbol{K}_{gab} \boldsymbol{K}_{gbb}^{-1} \boldsymbol{K}_{gba},$$

$$\overline{\boldsymbol{K}}_{fi} = \begin{bmatrix} \overline{\boldsymbol{K}}_{fi}^{(1)} & \overline{\boldsymbol{K}}_{fi}^{(2)} & \cdots & \overline{\boldsymbol{K}}_{fi}^{(6)} \end{bmatrix}_{18\times 6},$$

$\boldsymbol{\delta}_{ai} = \begin{pmatrix} \delta_{ai}^{(1)} & \delta_{ai}^{(2)} & \cdots & \delta_{ai}^{(6)} \end{pmatrix}_{6\times 1}^{\mathrm{T}}$.

In order to determine each column vector $\overline{\boldsymbol{K}}_{fi}^{(j)}$ in $\overline{\boldsymbol{K}}_f$, assign such that

$$\boldsymbol{\delta}_{ai} = \begin{pmatrix} 0 & \cdots & \underset{j}{1} & \cdots & 0 \end{pmatrix}_{6\times 1}^{\mathrm{T}}, \quad \boldsymbol{\delta}_{ak} = \mathbf{0}_{6\times 1}, \quad i = 1,2,3,$$
$$j = 1,\cdots,6, \quad k \neq i. \tag{47}$$

Then under the geometrical conditions given in eq. (47), $\boldsymbol{p}_a$ can be determined using a FEA software, leading to

$$\boldsymbol{p}_a \Rightarrow \overline{\boldsymbol{K}}_{fi}^{(j)}. \tag{48}$$

Hence, $\overline{\boldsymbol{K}}_f$ can finally be obtained by recycling subscripts i and j. It can be seen that 18 times computations are needed for this particular problem since there are 3 interface nodes between the limbs and machine frame.

5 Application

5.1 Stiffness evaluation

In order to demonstrate the effectiveness of the proposed modeling approach, let us define the translational (rotational) stiffness along (about) each axis at a point as the ratio of force (torque) against translational (rotational) deflection in that direction. Here, the stiffness of the TriVariant-B robot at point A_3 is evaluated in the spherical coordinate system $A_3 - x'y'z'$ defined in ref. [13]. The dimensional parameters of the SPM within the TriVariant-B robot are given in Table 1 and the component stiffness coefficients of the U$\underline{\text{P}}$S limb and the U limb are given in Tables 2—4 for the use of computer simulation. Figures 7(a)—(f) show the computed stiffness distribution in workspace S_t by considering simultaneously the compliances of the SPM and the machine frame. It can be seen that the stiffness at point A_3 along/about each axis is plane symmetrical due to the symmetry of the system structure and varies with the change of configurations. The translational stiffness along the z' axis is much higher than those along other two orthogonal axes and takes the minimum value at the centre of the workspace. On the contrary, the rotational stiffness about the z' axis takes the maximum value at the centre of the workspace. Distribution of the translational stiffness along the x' axis is similar to the rotational stiffness about the y' axis, while distribution of the translational stiffness along the y' axis is similar to the rotational stiffness about the x' axis.

Table 1 Dimension parameters of the TriVariant-B

a	b	r_3	ϕ	β
160 mm	500 mm	975 mm	12.56°	33°

Table 2 Axial stiffness of U$\underline{\text{P}}$S limb components (N/μm)

k_{a1}	k_{a2}	k_{a3}	k_{a4}	k_{a5}	k_{a6}	k_{a7}
910	989	115—126	312—1576	800	326	120

Table 3 Axial stiffness of U limb components (N/μm)

k_{ca1}	k_{ca2}
1580	102—113

Table 4 Torsional stiffness of U limb components (N.m/rad)×10^6

k_{ct1}	k_{ct2}
5.8	23.4—29.5

In order to identify, normally by means of sensitivity analysis, the influences of the component compliances on those of the system, partition the compliance matrix $\boldsymbol{C} = \boldsymbol{K}^{-1}$ such that $\boldsymbol{C} = (\boldsymbol{C}_p^{\mathrm{T}} \quad \boldsymbol{C}_\alpha^{\mathrm{T}})^{\mathrm{T}}$. Then, the following global performance indices are defined to evaluate the translational and rotational compliances of the system

$$\overline{\sigma}_{p(\alpha)} = \frac{\int_{S_t} \max\left(\sigma_{p(\alpha)}\right) \mathrm{d}s}{S}, \tag{49}$$

where $\max(\sigma_{p(\alpha)})$ is the maximum singular values of $\boldsymbol{C}_{p(\alpha)}$ and $\overline{\sigma}_{p(\alpha)}$ is its mean value throughout the workspace; S is the surface area of S_t.

Contributions of the component compliances in the SPM and the machine frame to the translational and rotational compliances of the system are shown in Table 5. It can be observed that the contributions of the compliance of the SPM to $\overline{\sigma}_p$ and $\overline{\sigma}_\alpha$ are 73% and 82%, and those of the machine frame are 27% and 18%, respectively. For the SPM itself, the component compliances in actuations have significant impact on $\overline{\sigma}_p$ (up to 42%), sequentially ordered by the U joint, S joint, rod, lead screw, etc; whilst the component compliances in constraints have significant impact on $\overline{\sigma}_\alpha$ (up to 53%), mainly due to the torsional compliance of the U limb.

5.2 Verification using FEA and experiments

On the basis of the above analysis, stiffness of the virtual prototype of the TriVariant-B was evaluated by ANSYS at three positions numbered by I—II within the workspace S_t shown in Figure 3. The FEA model at

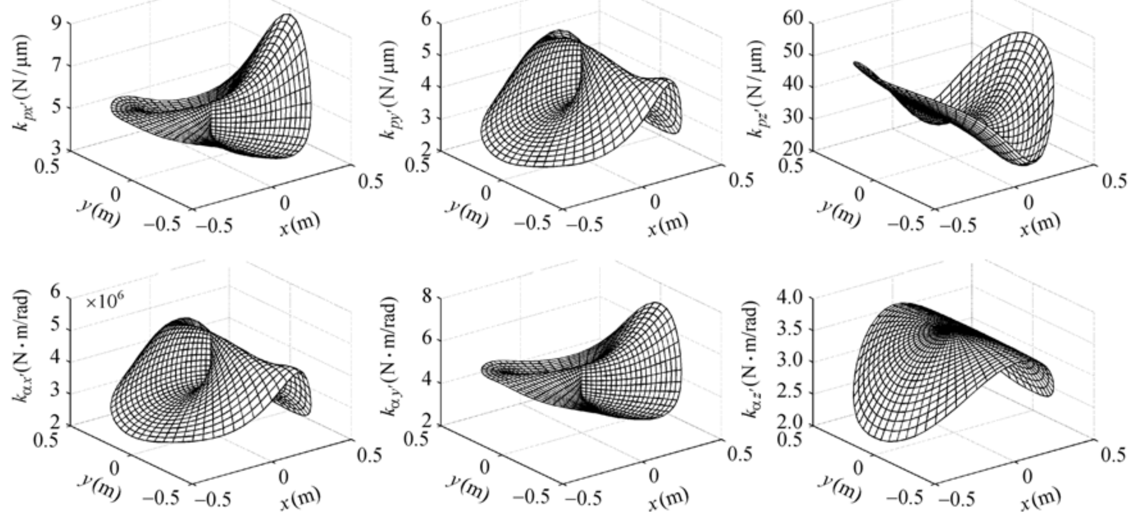

Figure 7 The stiffness distributions of the TriVariant-B in the workspace.

Table 5 Contributions of the component compliances in actuations and constraints (%)

	Frame	Component compliances in actuations							Component compliances in constraints					
	$\bar{\boldsymbol{K}}_f$	k_{a1}	k_{a2}	k_{a3}	k_{a4}	k_{a5}	k_{a6}	k_{a7}	k_{ca1}	k_{ca2}	k_{ct1}	k_{ct2}	$\boldsymbol{K}_{cb}$	$k_{Qu(v)}$
$\bar{\sigma}_p$	26.68	13.51	4.98	2.03	3.65	1.78	1.64	13.94	1.79	27.05	0.59	0.12	1.89	0.35
$\bar{\sigma}_\alpha$	17.91	9.44	3.48	1.42	2.56	1.24	1.14	9.73	1.15	17.38	26.06	5.30	2.70	0.49

Note: $\bar{\boldsymbol{K}}_f$, the component stiffness matrix of the machine frame; $k_{a1}-k_{a7}$, the axial stiffness coefficients of the components numbered 1−7 in the U<u>P</u>S limb; $k_{ca1(2)}$, the axial stiffness coefficient of the U limb body (U joint) at point A_3 along the w_3 axis; $k_{ct1(2)}$, the torsional stiffness coefficient of the U limb body (U joint) at point A_3 about the w_3 axis; $\boldsymbol{K}_{cb}$, the bending stiffness matrix of the U limb at point A_3 without considering the stiffness of the U joint; $k_{Qu(v)}$, the stiffness coefficients of the U joint of the U limb at point B_3 along the u_3 and v_3 axes.

position I is shown in Figure 8. It can be seen from Table 6 that the FEA results have a good match to those obtained by the analytical approach in terms of both magnitude, having discrepancy of less than 15%. The stiffness testing was also carried out on a prototype machine of the TriVariant-B robot shown in Figure 9. In the experiment, the force and displacement between the extremity of the limb and a base were read by dial indicators along with small movements of a jack shown in Figure 10. Then, difference between two readings of displacements with and without movement of the jack was taken as the deformation of the platform along that direction. This allows the stiffness to be determined using the mean value of a set of measurements. Table 6 shows that the experiments results also have a fairly good match to those obtained by the analytical approach, leaving 5%−30% discrepancy, due to the un-modeled contact stiffness.

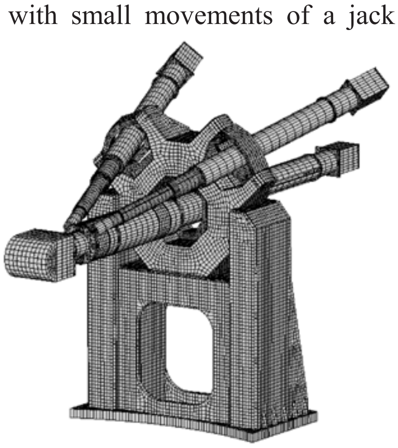

Figure 8 The FEA model.

Table 6 Stiffness comparisons

		Translational stiffness (N/μm)		
		Estimated	FEA	Tested
I	x'	3.87	3.65	3.53
	y'	5.63	5.51	5.43
	z'	31.5	27.0	20.3
II	x'	4.39	3.96	3.71
	y'	4.07	3.72	3.60
	z'	31.7	28.1	22.4

6 Conclusions

Taking the TriVariant-B robot as an object study, this

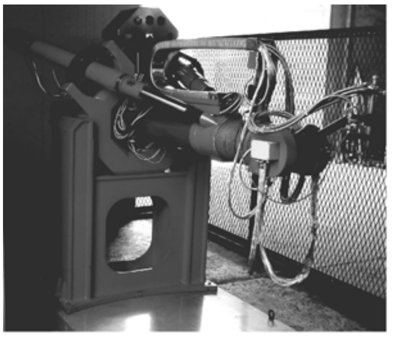

Figure 9 The TriVariant-B prototype.

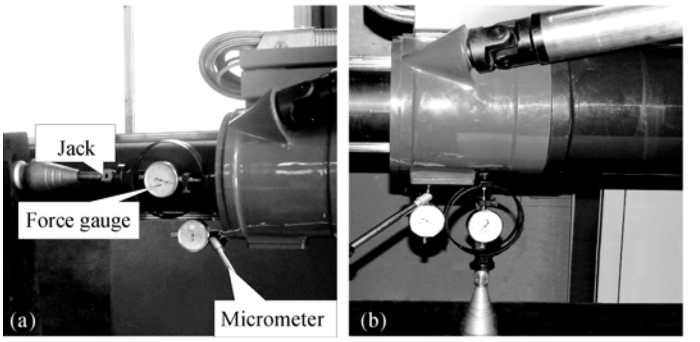

Figure 10 The stiffness measurement setups. (a) The vertical arrangement; (b) the horizontal arrangement.

paper presents a semi-analytical approach for the stiffness modeling of PKMs having the machine frame with complex geometry. The following conclusions are drawn:

(i) The modeling process can be implemented by: (1) stiffness modeling of one of two subsystems by assuming the other is rigid; (2) generation of the stiffness model of entire system by means of linear superposition.

(ii) The use of the overall deflection Jacobian allows the analytical stiffness model of the parallel mechanism to be formulated in an effective and compact manner by simultaneously taking into account the component compliances in both actuations and constraints.

(iii) The use of static condensation in structural mechanics allows the interface stiffness matrix between the parallel mechanism and machine frame to be determined using a commercialized FEA software.

(iv) Although only the TriVariant-B robot is considered as an example in this paper, the proposed modeling approach is so general that it can be applied to other PKMs having the machine frame with complex geometry.

1 Weck M, Staimer D. Parallel kinematic machine tools—Current states and future potentials. Ann CIRP, 2002, 51(2): 617－683

2 Gosselin C M. Stiffness mapping for parallel manipulators. IEEE Trans Rob Autom, 1990, 6(3): 377－382

3 Clinton C M, Zhang G. Stiffness modeling of a Stewart-platform-based milling machine. Trans NAMRI/ SME, 1997, 115: 335－340

4 EI-Khasawneh B S, Ferreira P M. Computation of stiffness and stiffness bounds for parallel link manipulators. Int J Mach Tool Manuf, 1999, 39: 321－342

5 Kim J, Park F C, Ryu S J, et al. Design and analysis of a redundantly actuated parallel mechanism for rapid machining. IEEE Trans Rob Autom, 2001, 17(4): 423－434

6 Tsai L W, Joski S. Kinematic analysis of 3-DOF position mechanisms for use in hybrid kinematic machines. Asme J Mech Des, 2002, 124(2): 245－253

7 Goldsmith P B, Design and kinematics of a three-legged parallel manipulator. IEEE Trans Rob Autom, 2003, 19(4): 726－731

8 Joshi S, Tsai L W. A Comparison study of two 3-DOF parallel manipulators: One with three and the other with four supporting legs. IEEE Trans Rob Autom, 2003, 19(2): 200－209

9 Zhang D, Gosselin C M. Kinetostatic modeling of N-DOF parallel mechanisms with a passive constraining leg and prismatic actuators. Asme J Mech Des, 2001, 123(3): 375－384

10 Zhang D, Gosselin C M. Kinetostatic modeling of parallel mechanisms with a passive constraining leg and revolute actuators. Mech Mach Theory, 2002, 37(6): 599－617

11 Zhang D, Gosselin C M. Kinetostatic analysis and design optimization of the Tricept machine tool family. Asme J Manuf Sci Eng, 2002, 124(3): 725－733

12 Wang Y Y, Huang T, Zhao X M, et al. Finite element analysis and comparison of two hybrid robots—The Tricept and the TriVariant. In: Proceedings of IEEE International Conference on Intelligent Robots and Systems, Beijing: IEEE, 2006. 490－495

13 Wang Y Y, Huang T, Derek G C, et al. An analytical method for stiffness modeling of the Tricept robot. Chin J Mech Eng (in Chinese), 2007, accepted

14 Corradini C, Fauroux J C, Krut S, et al. Evaluation of a 4-degree of freedom parallel manipulator stiffness. In: Proceedings of the 11th World Congress in Mechanism and Machine Science, Tianjin: IFFTOM, 2003, 5: 1857－1861

15 Rizk R, Munteanu M G, Fauroux J C, et al. A semi-analytical stiffness model of parallel robots from the Isoglide family via the sub-structuring principle. In: Proceedings of the 11th World Congress in Mechanism and Machine Science, Besançon: IFFTOM, 2007, 5: 623－628

16 Huang T, Zhao X Y, Whitehouse D J. Stiffness estimation of a tripod-based parallel kinematic machine. IEEE Trans Rob Autom, 2002, 18(1): 50－58

17 Huang T, Mei J P, Zhao X Y, et al. Stiffness estimation of a tripod-based parallel kinematic machine. In: Proceedings of IEEE International Conference on Robotics and Automation, Seoul: IEEE, 2001, 4: 3280－3285

18 Huang T, Li M, Zhao X M, et al. Conceptual design and dimensional synthesis for a 3-DOF module of the TriVariant—A novel 5-DOF reconfigurable hybrid robot. IEEE Trans Rob Autom, 2005, 21(3): 449－456

19 Liu H T, Huang T, Mei J P, et al. Kinematic design of a 5-DOF hybrid robot with large workspace/limb-stroke ratio. Asme J Mech Des, 2007, 129(5): 530－537

20 Joshi S, Tsai L W. Jacobian analysis of limited-DOF parallel manipulators. Asme J Mech Des, 2002, 124(2): 254－258